Progress In Electromagnetics Research C, Vol. 137, 139–153, 2023

Based on Fast Non-Singular Terminal Sliding of PMSM Model-Free Control

Yuxin Yang, Musheng Deng, Sicheng Li, and Yang Zhang*

Abstract—In model-free sliding mode control (MFSMC) of permanent magnet synchronous motor (PMSM), the first-order sliding mode surface convergence state is asymptotic convergence, and the dithering of the first-order sliding mode surface causes the motor control performance to degrade when the motor parameters change. To save the problem, a model-free fast non-singular terminal sliding mode control (MFFNTSMC) strategy is proposed. Firstly, considering the perturbation of motor parameters, a mathematical model of embedded permanent magnet synchronous motor is established, and the ultra-local model of the speed link is summarized. Then, according to the defined fast non-singular terminal sliding mode surface and the new reaching law, a new mode-free sliding mode controller based on the speed link is designed, which weakens the jitter by eliminating the high-gain switching by the high-order sliding surface, and at the same time makes the system state converge to zero in a limited time. In order to more accurately track the speed tracking effect, an extended sliding mode observer (ESMO) is used to observe the unknown disturbance of the system in real time. Finally, simulation and experiment comparisons with PI control as well as MFSMC control confirm that the method proposed in this paper has better steady state and transient performance for PMSM.

1. INTRODUCTION

PMSM is now widely used in various industrial drive systems as traction motors due to its good speed regulation performance, simple structure, high power factor, wide practical fields, and other advantages. At the same time, PMSM is a strongly coupled, nonlinear multivariable complex system [1–4]. In the face of sudden change in load torque or large fluctuations by external interference, due to the shortcomings of traditional proportional-integral (PI) saturation, it is difficult to meet the high-precision speed tracking of system speed using traditional PI control, and there is serious overshoot phenomenon at the initial start-up, resulting in the disadvantages of traditional PI control as a linear control strategy in the PMSM drive system, which cannot ensure the rapid and stable operation of the PMSM drive system in high-performance control applications [5].

In order to solve the limitations brought by traditional PI control, researchers have proposed a new control theory, which introduced nonlinear control into PMSM system variables, such as adaptive control [6–8], model prediction speed control [9–11], robust control [12–14], and sliding mode control [15–17]. Because sliding mode control is not easy to be interfered with by the outside world, it is widely used in PMSM control, but because the opening function is discontinuous, there will be serious oscillations at the critical point of the synovial surface, resulting in unstable system status. Therefore, the suppression of jitter in sliding mode control has become one of the research hotspots. Reference [17] introduced the use of a new reaching law to suppress jitter by varying the approach speed, but there is a problem that it does not converge in a finite time. Ref. [18] proposes a terminal synovial control method that converges the system state variables in a finite time, but there is a singular problem. Ref. [19] proposes that

Received 18 May 2023, Accepted 17 August 2023, Scheduled 4 September 2023
* Corresponding author: Yang Zhang (459387623@qq.com).
The authors are with the College of Electrical and Information Engineering, Hunan University of Technology, Zhuzhou 412007, China.

the application of fast terminal synovial membrane control in PMSM control can effectively solve the singular problem, but it has dependence on the mathematical model of the motor and does not consider the parameter mutation condition. Ref. [20] improving the approach law combined with the sliding mode observer effectively reduces the switching gain of the approach law and accurately compensates the disturbance, but it has dependence on the model. Based on the above control method, although it can effectively suppress the occurrence of overshoot and make the motor speed more accurately track the reference value, it is necessary to establish a high-precision system mathematical model as the basis, and the motor is complex in actual operation. It is difficult to achieve the ideal operating state, and the motor parameters may perturb under external disturbance [21]. Therefore, the above methods are very dependent on the system model and have some limitations.

In order to reduce the dependence of the system on the model, Mode-Free Control (MFC) is proposed [22]. By relying on the system inputs and outputs to establish a linkage without considering other parameter disturbances, the system is retained to contain the known terms of the parameters and the unknown terms of the system as the total disturbance values, so that the system parameter uptake does not affect the system itself, improving the system robustness and reducing the system dependence on the model. Reference [23] proposes a model-free parallel predictive torque control based on an ultra-local model, which reduces the dynamic adjustment process in the process of optimal voltage vector selection and improves the dynamic performance of the system. In [24], model-free sliding mode control is adopted in the speed of asynchronous motor, which improves the transient performance of the system and reduces the dependence on the model. Ref. [25] designs fractional order sliding mode without model control on the basis of fractional order theory, which improves the robustness of the system. Ref. [26] proposes a predictive current controller based on ultra-local model, which has good robustness to the existing unknown parameters and motor systems with coupled structures. Ref. [27] uses a mode-free sliding mode controller to achieve robust fault-tolerant control of the motor under magnetic loss fault, but does not analyse the influence of external disturbances on the system. Ref. [28] proposes to establish an extended state observer to observe unknown perturbations in the system, and through the comparison of different sampling frequencies, it is confirmed that the method has higher accuracy in tracking error. In [29], combined with sliding mode control, Model-Free Sliding Mode Control (MFSMC) is implemented by adopting the model-free control method in the PMSM speed link, which reduces the influence of motor parameter perturbation and external disturbance on the entire control system, but the system control adopts a first-order sliding mode surface, which makes the system state time converge asymptotically and affects the system state response speed.

To enhance the control effect of model-free sliding mode control in the case of parameter mutation in PMSM, this paper proposes a model-free fast non-singular terminal sliding mode control (MFFNTSMC) strategy. This method combines high-order sliding mode control and model-free control, while designing an extended sliding mode observer to observe the unknown disturbance of the system in real time. Finally, simulation and experiment comparisons with PI control as well as MFSMC control confirm that the method proposed in this paper has better steady state and transient performance for PMSM and improves the system control capability.

2. ULTRA-LOCAL MODE OF PMSM

In this paper, taking an interior PMSM as the research object, the stator core saturation, parameter disturbance, and hysteresis loss are ignored [3], and the mathematical model of PMSM in the *d-q* coordinate system is expressed as:

$$\begin{cases} u_d = R_s i_d + L_d \dfrac{di_d}{dt} - p_n \omega_m L_d i_q \\ u_q = R_s i_q + L_q \dfrac{di_q}{dt} + p_n \omega_m (L_q i_d + \psi_f) \\ T_e = 1.5 p_n i_q [i_d (L_d - L_q) + \psi_f] \\ \dfrac{d\omega_m}{dt} = \dfrac{1}{J}(T_e - B\omega_m - T_L) \end{cases} \tag{1}$$

where u_d, u_q are the component of the stator voltage in the d-q axis coordinate system; i_d, i_q are the component of the stator current in the d-q axis coordinate system; R_s is the nominal value of stator resistance; L_d, L_q are the inductance component in the d-q axis coordinate system; ψ_f is the nominal value of the permanent magnet flux linkage; ω_e is the mechanical angular velocity of the motor; p_n is the number of pole pairs of the motor; J is the moment of inertia; B is the coefficient of friction; T_e is electromagnetic torque; T_L is the load torque.

However, under the actual operating conditions of PMSM, the parameters contained in the motor system are perturbed by factors such as temperature and magnetic circuit saturation. Therefore, taking into account the perturbation of the system parameters, the mechanical equation of motion of the motor can be expressed as:

$$\frac{d\omega_m}{dt} = \frac{1}{J}[(T_e + \Delta T_e) - (B\omega_m + \Delta B\omega_m) - (T_L + \Delta T_L)] = \frac{1}{J}(T_e - B\omega_m - T_L) + \Delta d_\omega \tag{2}$$

where $\Delta d_\omega = (\Delta T_e - \Delta B\omega_m - \Delta T_L)/J$.

Substitute T_e into Equation (2)

$$\frac{d\omega_e}{dt} = 1.5\frac{p_n^2}{J}\psi_{ect} i_q - \frac{B}{J}\omega_e + \frac{p_n}{J}(\Delta d_\omega - T_L) \tag{3}$$

where $\omega_e = p_n\omega_m$ is the electric angular velocity of the motor. $\psi_{ect} = i_d(L_d - L_q) + \psi_f$ is a valid flux linkage.

By establishing its hyperlocal model of the single-input and single-output variables of the nonlinear system state, the known terms of the system parameters are retained as adjustable values, and the perturbations and external disturbances of the system parameters are classified as the total interference values, which can be expressed as:

$$\begin{cases} \dot{y} = \alpha u + F \\ y = x \end{cases} \tag{4}$$

where y, u are output and control inputs for the system; $x \in \Re$ is the system status value; $\dot{y}$ is the 1st derivative of y; α is the adjustable values for system parameters; F is the total interference value of the system.

According to Equation (3), the ultra-local model of the speed link of the IPMSM drive system can be obtained:

$$\frac{d\omega_e}{dt} = 1.5\frac{p_n^2}{J}\psi_{ect} i_q - \frac{R_\Omega}{J}\omega_e + \frac{p_n}{J}(\Delta d_\omega - T_L) = \alpha i_q + F \tag{5}$$

where $\alpha = 1.5p_n^2\psi_{ect}/J$ is an adjustable value for the q-axis current coefficient; $F = p_n(\Delta d_\omega - T_L)/J - B\omega_e/J$ is an unknown perturbated portion of the system.

According to the ultra-local model, the MFSM controller is designed by using the first-order sliding mode surface, and the sliding mode observer is used to observe the disturbance to form a mode-free sliding mode controller, and the framework is shown in Fig. 1.

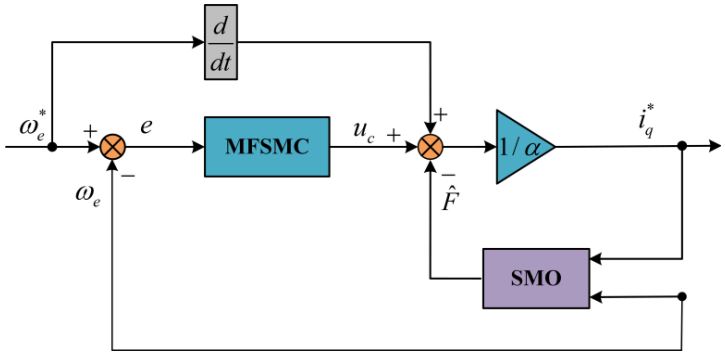

Figure 1. The framework diagram of MFSMC.

3. NEW REACHING LAW DESIGN

The design of sliding mode surface and reaching law is the key to sliding mode controller, and the selection of suitable sliding mode surface makes the system state variable close to the sliding mode surface under the influence of the proximity law. Through the designed reaching law, when the state variable is far from the sliding surface, it quickly responds to the sliding surface, and when it approaches the boundary point of the sliding mode, the response speed is close to zero; there is no overshoot.

Traditional exponential reaching law (TERL) can be expressed as:

$$\frac{ds}{dt} = -b_1 \mathrm{sgn}(s) - b_2 s \tag{6}$$

where $b_1 > 0$, $b_2 > 0$; s is the defined sliding surface; $b_1\mathrm{sgn}(s)$ is the isokinetic term; $b_2 s$ is the index item; $\mathrm{sgn}(s)$ is the symbolic function for sliding surfaces.

When $s > 0$, it can be obtained from Equation (1):

$$\frac{ds}{dt} = -b_1 - b_2 s \tag{7}$$

Equation (7) is obtained:

$$s(t) = -\frac{b_1}{k} + e^{-b_2 t} \tag{8}$$

Then the time for the sliding surface s to tend to zero is as follows:

$$t_{=}\frac{1}{b_2}\left\{\ln\left[s(0) + \frac{b_1}{k}\right] - \ln\frac{b_1}{k}\right\} \tag{9}$$

As can be seen from Equation (9) above, the smaller the b_1 value is and the larger the b_2 value is, the shorter the system response time is. However, increasing the b_2 value, the speed of the system response convergence to the sliding mode surface is enhanced, but due to the existence of the symbolic function, high-frequency oscillations are generated on the sliding mode surface, so the b_1, b_2 values need to be properly considered, so that the system response speed is fast, and the jitter is small.

In order to enhance the response speed of the system state and weaken the jitter, on the basis of the traditional approximation law, the relationship between the system state and the sliding mode surface is established by introducing the system state variable on the exponential term, and the continuous *Sigmoid* function $H(s)$ is used instead of the symbolic function.

A new exponential reaching law (NERL) is designed as follows:

$$\begin{cases} \dfrac{ds}{dt} = -c_1 N(s) H(s) - c_2 \left|x\right|^m s \\ H(s) = \dfrac{1 - e^{-s}}{1 + e^{-s}} \\ N(s) = \dfrac{1}{\dfrac{1}{l * |s| + 1} + \dfrac{1}{[\ln(|s| + 1) + m]^d}} \\ \lim\limits_{t \to \infty} |x| = 0 \end{cases} \tag{10}$$

where $c_1 > 0$, $c_2 > 0$, $l > 0$, $d > 0$, $m > 0$; s is the defined sliding face surfaces for the system; x is the state variable for the system. The regulating function $N(s)$ is added to the isokinetic term, and the system state variable $|x|^m$ is introduced as the regulating function in the exponential term. When the motion point of the system is infinitely far from the sliding surface, s and x tend to infinity, and the adjustment functions $N(s)$ and $|x|^m$ also tend to infinity, which accelerates the response speed of the system and makes it converge to the sliding mode surface quickly. When the motion point of the system is close to the sliding surface, s and x tend to be 0, then $N(s) = 1/(m+1)$ makes $c_1 N(s) < c_1$, reducing the system jitter.

The following nonlinear system is used to compare the performance of the traditional and new reaching laws [16]:

$$\begin{bmatrix} \dot{x}_1(t) \\ \dot{x}_2(t) \end{bmatrix} = \begin{bmatrix} 0 & 1 \\ 0 & -25 \end{bmatrix} \begin{bmatrix} x_1(t) \\ x_2(t) \end{bmatrix} + \begin{bmatrix} 0 \\ -133 \end{bmatrix} u \tag{11}$$

where $x_1(0) = 0$, $x_2(0) = 0$.

The design sliding surface is as follows:

$$s = 15x_1 + x_2 \tag{12}$$

Equation (12) can be derived:

$$\dot{s} = -133u - 10x_2 \tag{13}$$

The controller outputs of the traditional and new reaching laws are as follows:

$$\begin{cases} u_1 = -\dfrac{1}{133}(10x_2 - \varepsilon \mathrm{sgns} - ks) \\ u_2 = -\dfrac{1}{133}[10x_2 - \varepsilon N(s)H(x) - k\,|x|^m\, s] \end{cases} \tag{14}$$

The simulation effect of the two reaching laws is shown in Fig. 2 below.

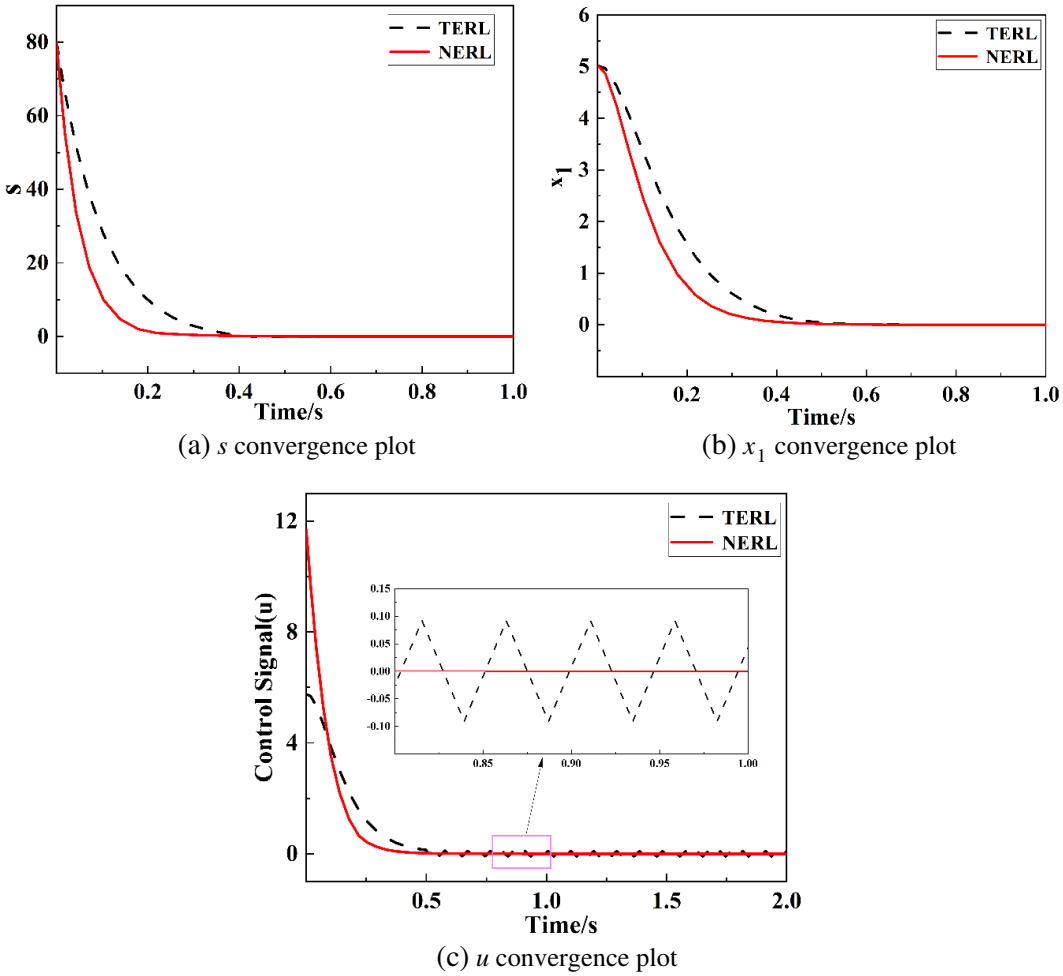

(a) s convergence plot

(b) x_1 convergence plot

(c) u convergence plot

Figure 2. Comparison of the performance of the two reaching laws.

Compared with the traditional exponential reaching law, it can be seen from (a), (b), and (c) in Fig. 2 that the jitter size of the traditional approximation rate is 0.19, while the jitter of the improved approximation rate is suppressed. The time when the sliding mode surface approaches to zero is faster than that of the traditional reaching rate, so the new reaching rate makes the system response speed change with the system change, strengthens the suppression effect of overshoot, weakens the jitter amplitude well, and enhances the adaptive ability of the system.

4. CONTROLLER DESIGN

4.1. Design of MFFNTSMC

To solve the problem that the model-free control of the first-order sliding mode surface of the IPMSM is reduced due to the change of parameters, this section combines the high-order sliding mode control and model-free control to design a new controller for the speed link.

According to Equation (5), combined with mode-free control, the controller of the speed link can be designed as:

$$i_q^* = \frac{\dot{\omega}_e^* - \hat{F} + u_c}{\alpha} \tag{15}$$

where ω_e^* is the given speed value of the motor; u_c is the output of the controller; $\hat{F}$ is observational estimates of perturbations.

Substitute Equation (15) into Equation (5):

$$u_c = -(\dot{\omega}_e^* - \dot{\omega}_e) \tag{16}$$

The motor speed error $e_\omega = \omega_e^* - \omega_e$ is defined as a system state variable, and the equation of state is designed as follows:

$$\begin{cases} \dot{e}_1 = e_2 \\ \dot{e}_2 = \dot{e}_\omega \end{cases} \tag{17}$$

For the above equation of state, the fast non-singular terminal sliding mode based on the high-order sliding form surface is designed as follows:

$$s = e_1 + \xi e_1^p + \gamma e_2^q \tag{18}$$

where $\xi > 0$, $\gamma > 0$ are state error gains; $1 < q < 2$, $p > q$ are positive odd numbers.

When $s = 0$, the resulting equation is as follows:

$$e_2 = e_\omega = -\left[\frac{1}{\gamma}\left(e_1 + \xi e_1^p\right)\right]^{\frac{1}{q}} = \sigma\left(e_1 + \xi e_1^p\right)^{\frac{1}{q}} \tag{19}$$

where $\sigma = -\left(1/\gamma\right)^{1/q}$, $\sigma < 0$.

Suppose that in finite time t seconds, the system converges to zero, integrating both sides of Eq. (19):

$$\begin{aligned} \int_{e0}^{e1} de_1 &= \int_0^t \sigma\left(e_1 + \xi e_1^p\right)^{\frac{1}{q}} dt \\ \int_{e0}^{e1} \frac{1}{e_1^q} de_1 &= \int_0^t \sigma\left(1 + \xi e_1^{p-1}\right)^{\frac{1}{q}} dt \end{aligned} \tag{20}$$

where $1 \le (1 + \xi e_1^{p-1})$, $\sigma < 0$, the following inequality is obtained:

$$\int_{e0}^{e1} \frac{1}{e_1^q} de_1 \;\; \le \int_0^t \sigma dt \le -\int_0^t \left(\frac{1}{\gamma}\right)^{1/q} dt \tag{21}$$

the results are as follows:

$$t \le \frac{\gamma^{1/q}}{1-q} e_1(0)^{1-q} \tag{22}$$

From Equation (22), it can be seen that when the appropriate parameters are selected, the system state variable will converge to zero along the sliding die surface for a limited time.

Taking Equation (18) for derivation:

$$\dot{s} = \dot{e}_1 + \xi p e_1^{p-1}\dot{e}_1 + \gamma q e_2^{q-1}\dot{e}_2 = e_2 + \xi p e_1^{p-1} e_2 + \gamma q e_2^{q-1}\dot{e}_2 \tag{23}$$

When $\dot{s} = 0$, the equivalent control law u_e is obtained:

$$u_e = \left(\frac{1}{\gamma q}\right)\left(e_2 + \xi p e_2^{p-1}\right) = \left(\frac{1}{\gamma q}\right) e_2^{2-q}\left(1 + \xi p e_2^{p-2}\right) \tag{24}$$

In order to accelerate the speed of the state variable reaching the higher-order sliding surface, a new model-free controller u_c based on the fast non-singular terminal sliding mode can be obtained using the new exponential approximation law of Equation (10) and the higher-order sliding face of combined Eq. (18):

$$u_c = u_e + c_1 N(s) H(s) c_2 + |\mathrm{e}_\omega|^m s \tag{25}$$

Select the Lyapunov function V to prove that the designed controller is stable.
The proof is as follows:

$$V = 0.5 e_1^2 \tag{26}$$

Taking Equation (26) for derivation:

$$\begin{aligned}
\dot{V} &= \mathrm{e}_1 \dot{e}_1 \\
&= e_1 e_2 \\
&= e_1 \sigma \left(e_1 + \xi e_1^p\right)^{\frac{1}{q}} \\
&= \sigma \left(e_1^{q+1} + \xi e_1^{q+p}\right)^{\frac{1}{q}} \\
&= \sigma \left(2V e_1^{q-1} + 2V \xi e_1^{p+q-2}\right)^{\frac{1}{q}} \\
&= \sigma (2V)^{1/q} \cdot e_1^{1-1/q} (1 + \xi e_1^{p-1})^{\frac{1}{q}}
\end{aligned} \tag{27}$$

when $1 < q < 2$, $p > q$ satisfying Equation (28).

$$1 - \frac{1}{q} = \frac{q-1}{q} = \frac{2a}{q}, \ (a = 1, 2, 3, \ldots) \tag{28}$$

the following results can be obtained:

$$\begin{aligned}
\dot{V} &= \sigma (2V)^{\frac{l}{k}} \cdot e_1^{\frac{2a}{q}} (1 + \xi e_1^{\frac{2b}{h}})^{\frac{l}{k}} \\
&\leq \sigma (2V)^{\frac{l}{k}} \cdot e_1^{\frac{2a}{q}} \\
&\leq 0
\end{aligned} \tag{29}$$

According to *Lyapunov* of stability theorem, the system state can converge to zero in a finite amount of time depending on the slip. The approximation law can follow the adaptive adjustment speed of the system state variable to converge at FNTSM. According to Equation (18), the exponential terms are all positive and have $0 < 2 - p < 0$, thus avoiding the singular problem of control. Due to the continuous symbol term in the controller, jitter is suppressed, and the convergence time of the system state is reduced. Through Equation (22) it is known that the systematic state error will converge to zero in finite time. According to Equation (29) we know that $\dot{V} \leq 0$, which satisfies the *Lyapunov* of stability theorem, so the designed controller is stable. The control block diagram is shown in Fig. 3 below.

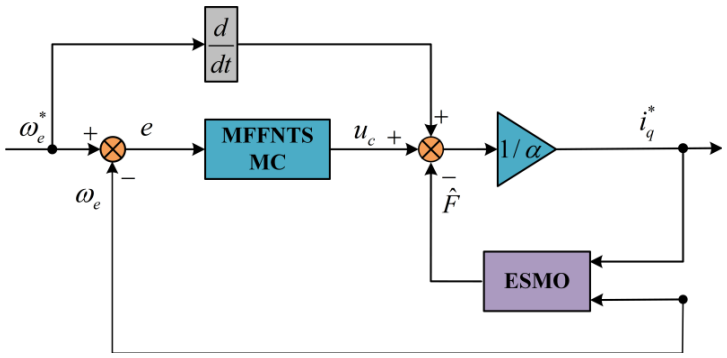

Figure 3. The framework diagram of MFFNTSMC.

Equation (15) and Equation (25) are combined to obtain Equation (30):

$$i_q^* = \frac{\dot{\omega}_e^* - \hat{F} + u_c}{\alpha} = \frac{\dot{\omega}_e^* - \hat{F} + \left(\frac{1}{\gamma q}\right) e_\omega^{2-q}\left(1 + \xi p e_\omega^{p-2}\right) + c_1 N(s) H(s) + c_2 \left|\mathrm{e}_\omega\right|^m s}{\alpha} \tag{30}$$

4.2. Extended Sliding Observer Design

In order to improve the immunity performance of the controller, this section introduces a method based on the extended synovial disturbance observer [30], using the unknown perturbation value F as the extended variable of the system, so the extended sliding mode observer (ESMO) is designed.

The ultra-model matrix form of PMSM speed link based on extended variable F is established.

$$\begin{bmatrix} \dot{\omega}_\mathrm{e} \\ \dot{F} \end{bmatrix} = \begin{bmatrix} 0 & 1 \\ 0 & 0 \end{bmatrix} \begin{bmatrix} \omega \\ F \end{bmatrix} + \begin{bmatrix} \alpha \\ 0 \end{bmatrix} i_q + \begin{bmatrix} 0 \\ 1 \end{bmatrix} f(t) \tag{31}$$

where $f(t)$ is the rate of change of the unknown perturbation F.

In order to measure the unknown disturbance, the design observer is:

$$\begin{bmatrix} \dot{\hat{\omega}}_\mathrm{e} \\ \dot{\hat{F}} \end{bmatrix} = \begin{bmatrix} 0 & 1 \\ 0 & 0 \end{bmatrix} \begin{bmatrix} \hat{\omega} \\ \hat{F} \end{bmatrix} + \begin{bmatrix} \alpha \\ 0 \end{bmatrix} i_q + \begin{bmatrix} 1 \\ g \end{bmatrix} u_{smo} \tag{32}$$

where $\hat{\omega}_\mathrm{e}$ is the estimate of the observation of ω_e; $\hat{F}$ is the estimate of the observed perturbation; u_{smo} is the function to be designed; g is the function gain value.

Subtract Equation (32) from Equation (31):

$$\begin{cases} \dot{e}_\omega = \dot{\omega}_e - \dot{\hat{\omega}}_e = F - \hat{F} - u_{smo} \\ \dot{e}_F = \dot{F} - \dot{\hat{F}} = f(t) - g u_{smo} \end{cases} \tag{33}$$

where e_ω is the difference between the given value of the rotational speed and the observed actual value; e_F is the unknown perturbation observation error in the rotational speed part.

The sliding surface is designed as $s_1 = e_\omega$, and the exponential reaching law is substituted into Equation (33).

$$e_F - u_{smo} = -k_1 \mathrm{sgn}(e_\omega) - k_2 e_\omega \tag{34}$$

In Equation (34), e_F is part of the unknown perturbation observation, so u_{smo} can be expressed as:

$$u_{smo} = k_1 \mathrm{sgn}(e_\omega) + k_2 e_\omega \tag{35}$$

Let $V_1 = 0.5 s_1^2$ prove the stability of the observer as a Lyapunov function, as shown below:

$$\begin{aligned} \dot{V} &= s_1 \dot{s}_1 \\ &= e_\omega \dot{e}_\omega \\ &= e_\omega \left(e_F - U_{smo}\right) \\ &= e_\omega \left(-k_1 \mathrm{sgn}(e_\omega) - k_2 e_\omega\right) \le 0 \end{aligned} \tag{36}$$

and from the *Lyapunov* stability judgment, it can be seen that the difference between the given value of the rotational speed and the actual observed value will converge to zero at a reasonable value, and the designed observer tends to be stable.

In summary, the framework of the PMSM system based on MFFNTSMC in this paper is shown in Fig. 4.

5. SIMULATION AND EXPERIMENTATION

To prove the superiority of the proposed method in the control of permanent magnet synchronous motor drive system compared with PI control and mode-free control using first-order sliding surface, MATLAB simulation and RT-LAB semi-physical experiment are used to verify.

The PMSM drive system control strategy is to use Maximum Torque per Ampere (MTPA) control. Table 1 shows the parameters of PMSM, and Table 2 shows the controller parameters of the three control schemes.

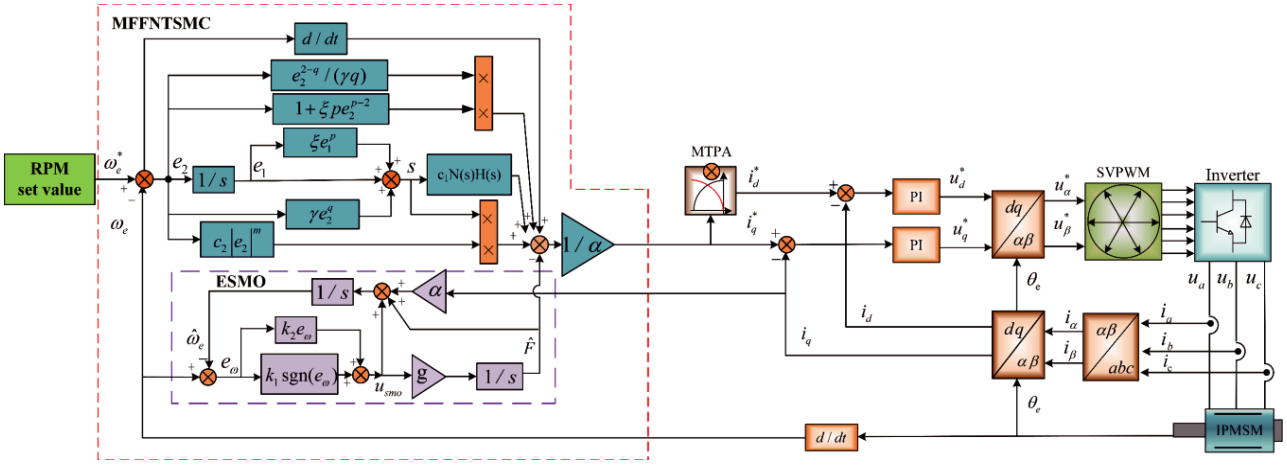

Figure 4. The framework diagram of the PMSM system.

Table 1. Motor parameters.

Parameter name	Unit	Values
Rated power/P_N	KW	6.6
Rated speed/n_N	$r/\min$	3000
DC voltage/u_{dc}	V	311
Stator resistance/R_s	Ω	0.025
q axis inductance/L_q	H	0.00047
d axis inductance/L_d	H	0.0002
Magnetic flux/ψ_f	Wb	0.062
Pole number/p_n	pairs	4
Inertia/J	$\mathrm{kg}\cdot\mathrm{m}^2$	0.01
Damping factor/B	$\mathrm{Nm}\cdot\mathrm{s/rad}$	0.001

Table 2. Controller parameters.

Control schemes	Values
The first: PI	$K_I = 800,\ K_P = 15$
The second: MFSMC	$c = 300,\ b_1 = 0.2,\ b_2 = 0.001$
	$c_1 = 0.2,\ c_2 = 0.01,\ m = 0.2$
The third: MFFNTSMC	$d = 10,\ l = 300,\ \gamma = 100$
	$q = 2.8,\ p = 1.5,\ \xi = 200$

5.1. System Simulation Analysis

Initially, the motor is started with $5\,\mathrm{N}\cdot\mathrm{m}$ load, and the speed is given at $100\,\mathrm{r/min}$; at $0.5\,\mathrm{s}$, the motor speed rises from $1000\,\mathrm{r/min}$ to $2000\,\mathrm{r/min}$; at $1\,\mathrm{s}$, the load is increased suddenly, so that the load torque increases from $5\,\mathrm{N}\cdot\mathrm{m}$ to $15\,\mathrm{N}\cdot\mathrm{m}$; at $1.5\,\mathrm{s}$, the stator resistance of $0.025\,\Omega$ is mutated to $0.1\,\Omega$; at $2\,\mathrm{s}$, the stator q-axis inductance of $0.00047\,\mathrm{H}$ is suddenly increased to $0.00147\,\mathrm{H}$; at $2.5\,\mathrm{s}$, the stator d-axis inductance of $0.0002\,\mathrm{H}$ is suddenly increased to $0.0005\,\mathrm{H}$. The simulation results of the three control

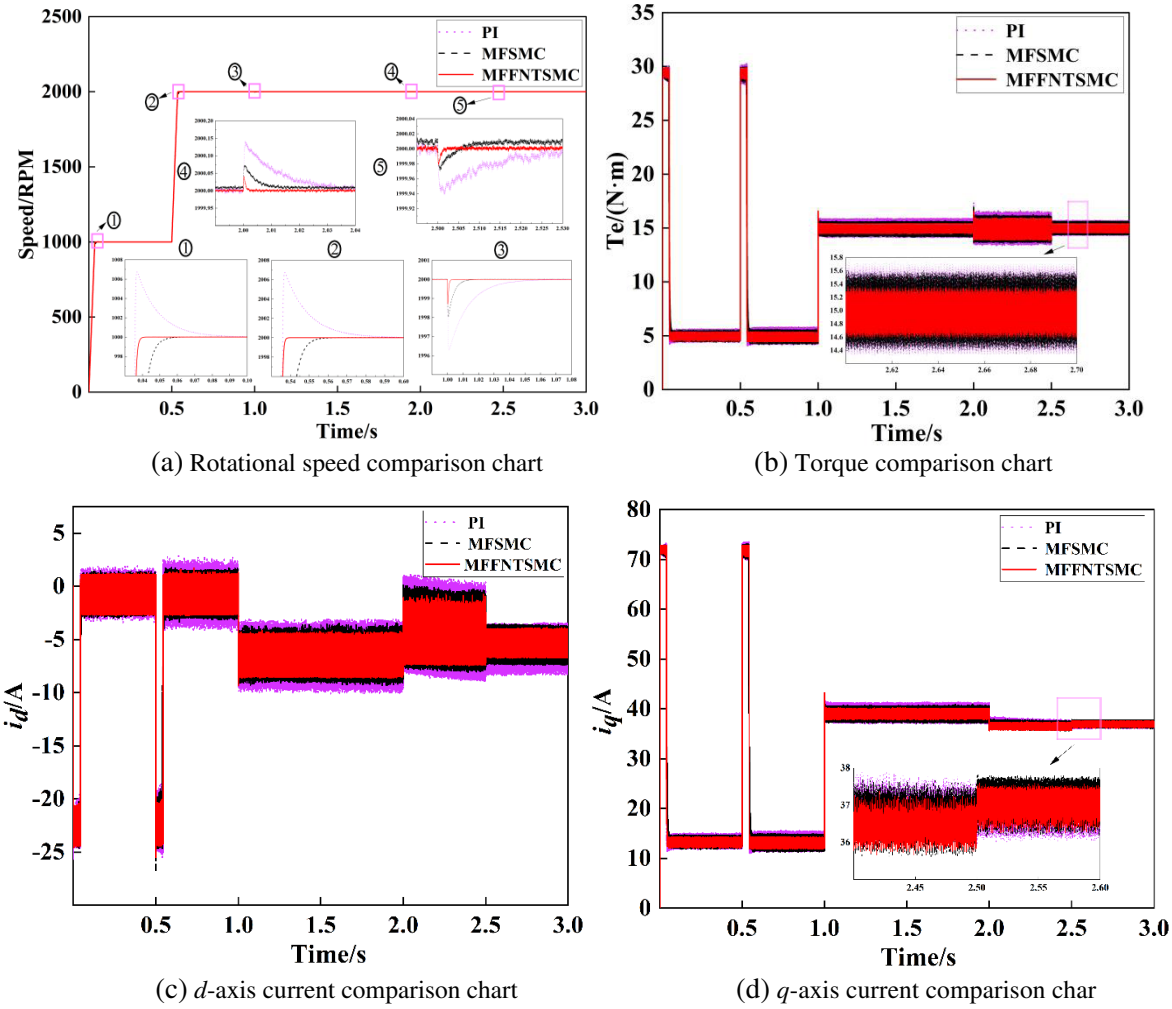

(a) Rotational speed comparison chart

(b) Torque comparison chart

(c) d-axis current comparison chart

(d) q-axis current comparison char

Figure 5. Three control operating condition diagrams.

schemes with perturbed motor parameters are shown in Fig. 5.

From the speed simulation graph in Fig. 5(a), it can be seen that the motor is initially started with load to 1000 r/min. The first control has overshoot, and overshoot reaches 1006.7 r/min. The second control and third control have no overshoot. The first control reaches the given value in 0.1 s. The second control reaches the given value in 0.06 s, and the third control takes only 0.04 s to reach the given value. When the speed rises to 2000 r/min at 0.5 s, the first control overshoots to 2006.68 r/min and reaches stability at 0.62 s; the second control reaches stability at 0.57 s; and the third control reaches stability at 0.54 s. When the load torque increases suddenly at 1 s, the first control drops to 1996.3 r/min and returns to stability at 1.06 s. The second control decreases to 1998.1 r/min, and stabilization is restored at 1.018 s. The third control decreases to 1998.7 and resumes stability at 1.004 s. When the d-axis and q-axis inductance values change, the first and second controllers experience significant overshoot and much longer recovery times than the third controller. The speed accuracy of the third control is better than the first two controls under sudden changes in motor parameters.

From Figs. 5 (a), (b), (c), and (d), it can be seen that under the three control schemes, the effect on motor performance is almost negligible in the face of stator resistance changes, and the motor torque, d-axis current, and q-axis current under the third control are superior, less current fluctuation, and more accurate speed than the first two controls in the face of sudden changes in load torque and sudden increases in d-axis and q-axis inductance.

Fig. 6 shows the total harmonic distortion (THD) analysis of the stator current i_a under the three

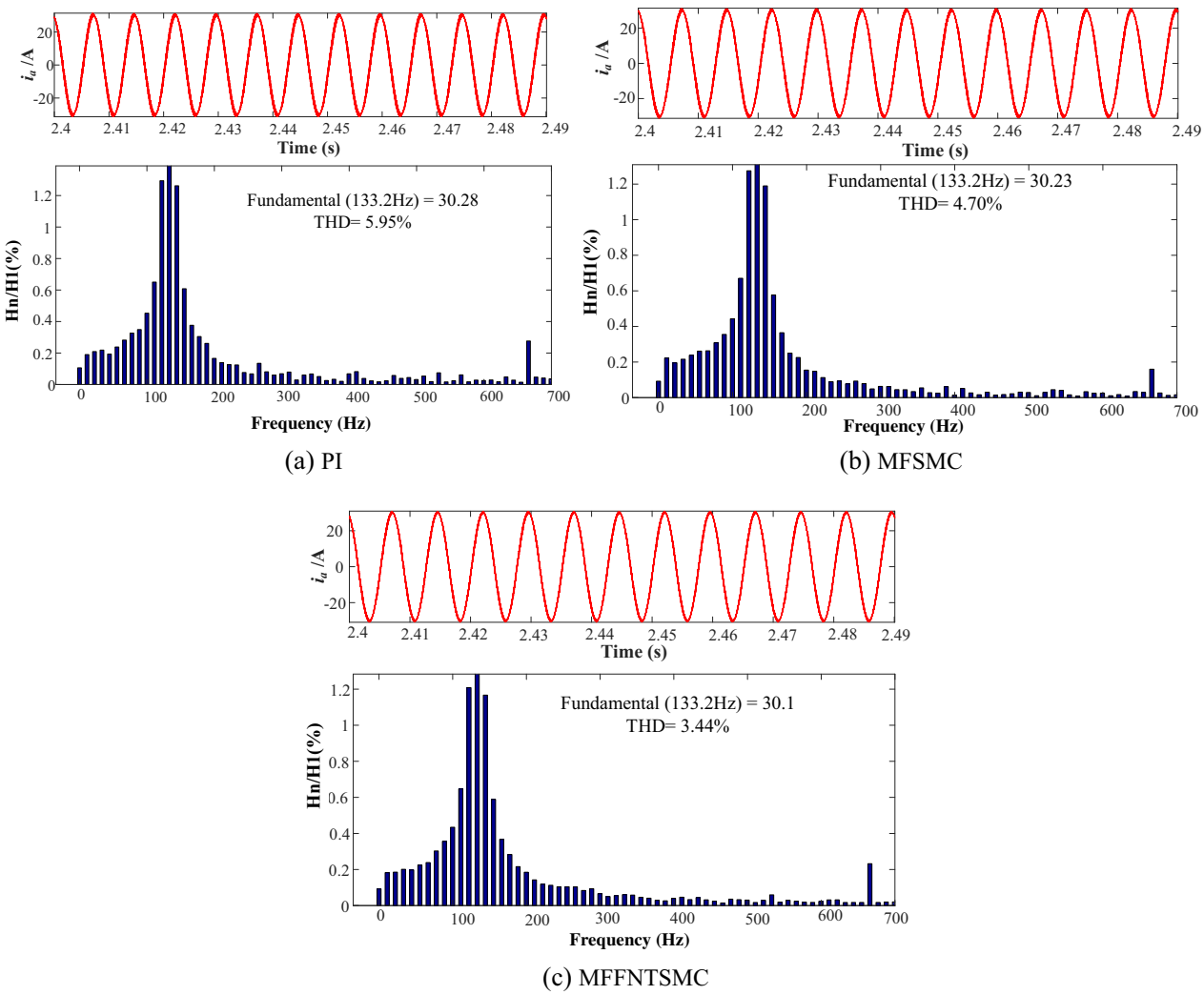

Figure 6. Total harmonic distortion rate of current i_a for the three control cases.

control methods. The THD is 5.59% and 4.7% for PI control and MFSMC, respectively, while it is further reduced to 3.44% when MFFNTSMC is used. It can be seen that MFFNTSMC is insensitive to system parameter changes, thus providing better suppression of current harmonics and effectively ensuring the anti-disturbance capability of the motor under parameter changes.

The THD analysis of the stator current for the three control methods is shown in Fig. 6.

5.2. System Experimental Analysis

This paper further verifies the effectiveness of the control method proposed in this paper through RT-LAB experiments. Fig. 7 shows the diagram of the RT-LAB semi-physical simulation experimental platform used in this paper. Fig. 7(a) shows the experimental platform. The digital signal processing (DSP) model used for the controller is TMS320F2812, and the PMSM driver part is constructed using OP5600. Fig. 7(b) shows the in-loop configuration, setting up the test and simulation environment consistently.

Fig. 8 shows the experimental graphs corresponding to the three control methods, and the motor operating conditions in the experiment and the motor operating conditions in the simulation are the same. The first control method uses PI; the second control method uses MFSMC; and the third method uses MFFNTSMC.

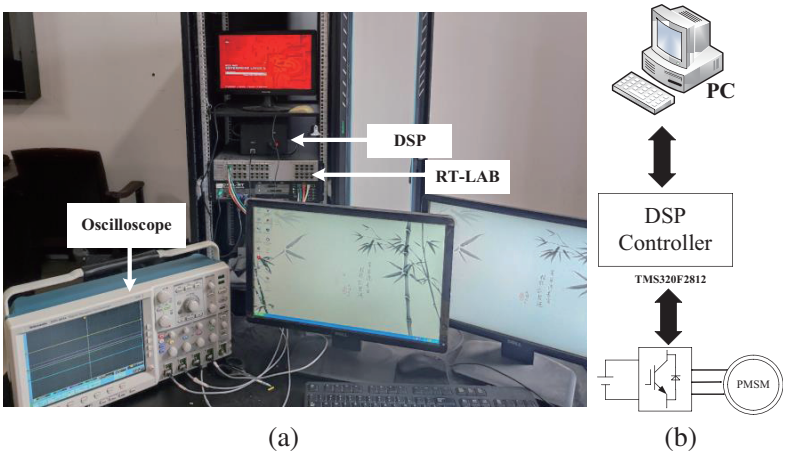

Figure 7. RT-LAB semi-physical simulation experiment platform diagram.

From Figs. 8(a), (b), and (c), the different performances of PMSM use three control methods under the same operating conditions. When the initial value is given to start with load, watching the torque it can be learned that there is overshooting in the PI control, no overshooting in the MFSMC and MFFNTSMC, and the MFFNTSMC reaches the stabilization faster. When the motor is running for 0.5 s, the PMSM boost speed reaches 2000 r/min; the MFFNTSMC returns to stability faster; and the d-q axis current and torque fluctuations are smaller. When the load changes from $5\,\mathrm{N}\cdot\mathrm{m}$ to $15\,\mathrm{N}\cdot\mathrm{m}$ at 1 s, the torque and current fluctuations of PI control and MFSMC are not as stable as those of MFFNTSMC. When the motor is running for 1.5 s, the resistance changes from $0.025\,\Omega$ to $0.1\,\Omega$, and it can be seen from the torque that the MFFNTSMC is more robust to sudden changes in resistance. When the motor is running for 2 s, the resistance changes suddenly. When 2 s, the motor q-axis inductance changes from 0.00047 H to 0.00147 H, and from the graph of q-axis current, it can be learned that the motor q-axis current fluctuates less under the control of MFFNTSMC when the q-axis inductance changes abruptly. When the motor is running for 2.5 s, the motor d-axis inductance changes from 0.0002 H to 0.0005 H. From the d-axis current graph, it is known that the motor d-axis current fluctuates less under MFFNTSMC control. Therefore, the first control method and second control method have larger d-q axis current and torque fluctuations when the motor parameters change and larger speed fluctuations when the parameters change abruptly.

Compared with the first two methods, the third control method has smaller fluctuations in d-q-axis current and torque and faster speed response when the parameters change abruptly, which improves the anti-interference performance of the system and makes the motor system superior. The specific control performance index data of the three control methods are shown in Table 3 below.

Table 3 shows the performance comparison under the three control methods. From the initial response speed, given the initial value, the time taken to stabilize the motor operation is 0.1 s for PI control, 0.06 s for MFSMC and 0.04 s for MFFNTSMC from the harmonic distortion rate of A-phase current. THD is 5.59% for PI control, 4.7% for MFSMC, and 3.44% for MFFNTSMC from the torque pulsation, and it is 9.1% for PI control, 7.3% for MFSMC, and 4.6% for MFFNTSMC 9.1%. MFSMC is 7.3%, and MFFNTSMC is 4.6%. Therefore, by comparing the performances under three control methods, MFFNTSMC control has the best performance.

Table 3. Comparison of performance under three types of control.

Performance Indicators	The first: PI	The second: MFSMC	The third: MFFNTSMC
Initial speed response/s	0.10	0.06	0.04
i_a THD/%	5.95	4.7	3.44
Torque pulsation/%	9.1	7.3	4.6

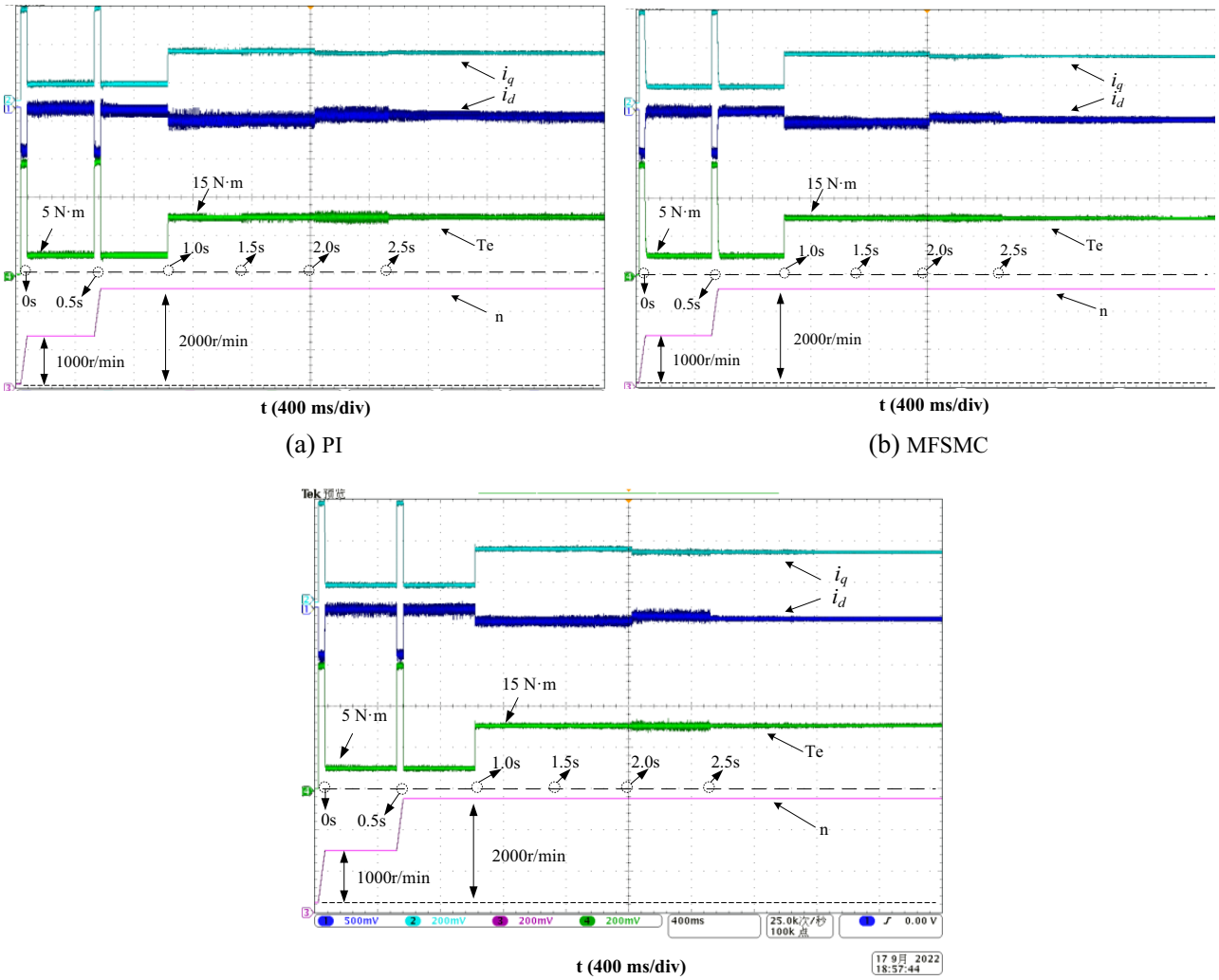

Figure 8. Experimental diagram of three control methods.

6. CONCLUSION

To solve the problem of motor control performance degradation due to parameter changes when model-free control with first-order sliding mode is used in the speed link of PMSM, a fast non-singular terminal sliding mode model-free control strategy is proposed in this paper. Firstly, an ultra-local model is established to replace the speed ring mathematical model of permanent magnet synchronous motor under unknown perturbation disturbance. Then, a new convergence law is designed based on the principle of the traditional exponential convergence law, which is combined with a fast non-singular terminal sliding mode surface to design a model-free fast non-singular terminal sliding mode control (MFFNTSMC) based on speed ring. Secondly, for more accurate speed tracking effect, an extended sliding mode observer (ESMO) is designed to observe the unknown disturbances of the system in real time. Finally, comparing the simulation and experimental data with PI control and MFSMC control under the same operating conditions, the following conclusions can be drawn:

(1) The MFFNTSMC controller, compared to the previous two controllers, reduces the convergence time of the state variables of the system so that the motor starts initially without overshoot and reaches the given speed quickly.

(2) Compared with PI and MFSMC, the proposed control method reduces the A-phase current THD to 3.44% and the torque pulsation to 4.6%, which has better steady-state performance.

(3) The control method proposed in this paper further enhances the transient performance and response speed of model-free sliding mode control during the sudden increase of motor torque and sudden change of *d-q* axis inductance, which enhances the control effect of the system and guarantees the stability of the system under high performance operation.

In this paper, the effect of permanent magnet chain variation on the proposed method has not been considered, which will be focused on in the next step.

ACKNOWLEDGMENT

This work was supported by the Natural Science Foundation of Hunan Province of China under Grant Number 2023JJ50191 and Educational Commission of Hunan Province of China under Grant Number 21B0552.

REFERENCES

1. Bai, C., Z. Yin, Y. Zhang, and J. Liu, "Robust predictive control for linear permanent magnet synchronous motor drives based on an augmented internal model disturbance observer," *IEEE Transactions on Industrial Electronics*, Vol. 69, No. 10, 9771–9782, 2022.
2. Fan, Z.-X., S. Li, and R. Liu, "ADP-based optimal control for systems with mismatched disturbances: A PMSM application," *IEEE Transactions on Circuits and Systems II: Express Briefs*, Vol. 70, No. 6, 2057–2061, Jun. 2023.
3. Ullah, K., J. Guzinski, and A. F. Mirza, "Critical review on robust speed control techniques for permanent magnet synchronous motor (PMSM) speed regulation," *Energies*, Vol. 15, No. 3, 1235, 2022.
4. Pang, D.-C., Z.-J. Shi, Y.-H. Chang, H.-C. Huang, and G.-T. Bui, "Investigation of an interior micro permanent magnet synchronous motor," *Energies*, Vol. 14, No. 14, 4172, 2021.
5. Zhao, K., et al., "Demagnetization-fault reconstruction and tolerant-control for PMSM using improved SMO-based equivalent-input-disturbance approach," *IEEE/ASME Transactions on Mechatronics*, Vol. 27, No. 2, 701–712, 2022.
6. Wu, J., J. Zhang, B. Nie, Y. Liu, and X. He, "Adaptive control of PMSM servo system for steering-by-wire system with disturbances observation," *IEEE Transactions on Transportation Electrification*, Vol. 8, No. 2, 2015–2028, Jun. 2022.
7. Qiu, H., H. Zhang, L. Min, T. Ma, and Z. Zhang, "Adaptive control method of sensorless permanent magnet synchronous motor based on super-twisting sliding mode algorithm," *Electronics*, Vol. 11, No. 19, 3046, 2022.
8. Novak, Z. and M. Novak, "Adaptive PLL-based sensorless control for improved dynamics of high-speed PMSM," *IEEE Transactions on Power Electronics*, Vol. 37, No. 9, 10154–10165, Sept. 2022.
9. Yi, P., X. Wang, D. Chen, and Z. Sun, "PMSM current harmonics control technique based on speed adaptive robust control," *IEEE Transactions on Transportation Electrification*, Vol. 8, No. 2, 1794–1806, 2022.
10. Wei, Y., Y. Wei, Y. Sun, H. Qi, and M. Li, "An advanced angular velocity error prediction horizon self-tuning nonlinear model predictive speed control strategy for PMSM system," *Electronics*, Vol. 10, No. 9, 1123, 2021.
11. Li, Z., F. Wang, D. Ke, J. Li, and W. Zhang, "Robust continuous model predictive speed and current control for PMSM with adaptive integral sliding-mode approach," *IEEE Transactions on Power Electronics*, Vol. 36, No. 12, 14398–14408, 2021.
12. Jiang, W., W. Han, L. Wang, Z. Liu, and W. Du, "Linear golden section speed adaptive control of permanent magnet synchronous motor based on model design," *Processes*, Vol. 10, No. 5, 1010, 2022.

13. Duan, J., S. Wang, and L. Sun, "Backstepping sliding mode control of a permanent magnet synchronous motor based on a nonlinear disturbance observer," *Applied Sciences*, Vol. 12, No. 21, 11225, 2022.
14. Li, S., Y. Xu, W. Zhang, and J. Zou, "Robust deadbeat predictive direct speed control for PMSM with dual second-order sliding-mode disturbance observers and sensitivity analysis," *IEEE Transactions on Power Electronics*, Vol. 38, No. 7, 8310–8326, Jul. 2023.
15. Xu, B., L. Zhang, and W. Ji, "Improved non-singular fast terminal sliding mode control with disturbance observer for PMSM drives," *IEEE Transactions on Transportation Electrification*, Vol. 7, No. 4, 2753–2762, 2021.
16. Fu, D. and X. Zhao, "A novel robust adaptive nonsingular fast integral terminal sliding mode controller for permanent magnet linear synchronous motors," *IEEE Journal of Emerging and Selected Topics in Power Electronics*, Vol. 11, No. 2, 1672–1683, Apr. 2023.
17. Jiang, C., Q. Wang, Z. Li, N. Zhang, and H. Ding, "Nonsingular terminal sliding mode control of PMSM based on improved exponential reaching law," *Electronics*, Vol. 10, No. 15, 1776, 2021.
18. Rafiq, M. A., A. Ulasyar, W. Uddin, H. S. Zad, A. Khattak, and K. Zeb, "Design and control of a quasi-Z source multilevel inverter using a new reaching law-based sliding mode control," *Energies*, Vol. 15, No. 21, 8002, 2022.
19. Lin, F.-J., S.-G. Chen, M.-S. Huang, C.-H. Liang, and C.-H. Liao, "Adaptive complementary sliding mode control for synchronous reluctance motor with direct-axis current control," *IEEE Transactions on Industrial Electronics*, Vol. 69, No. 1, 141–150, 2022.
20. Xu, D., B. Ding, B. Jiang, W. Yang, and P. Shi, "Nonsingular fast terminal sliding mode control for permanent magnet linear synchronous motor via high-order super-twisting observer," *IEEE Transactions on Mechatronics*, Vol. 27, No. 3, 1651–1659, 2022.
21. Yue, Y., Y. Geng, and W. Wang, "Continuous nonsingular fast terminal sliding mode control for speed tracking of PMSM based on finite time disturbance observer," *Processes*, Vol. 10, No. 7, 1407, 2022.
22. Jiang, C., Q. Wang, N. Zhang, and H. Ding, "Overcurrent protection and unmatched disturbance rejection under non-cascade structure for PMSM," *Energies*, Vol.15, No. 18, 6573, 2022.
23. Li, T. and X. Liu, "Model-free non-cascade integral sliding mode control of permanent magnet synchronous motor drive with a fast reaching law," *Symmetry*, Vol. 13, No. 9, 1680, 2021.
24. Lv, M., S. Gao, Y. Wei, D. Zhang, H. Qi, and Y. Wei, "Model-free parallel predictive torque control based on ultra-local model of permanent magnet synchronous machine," *Actuators*, Vol. 11, No. 2, 31, 2022.
25. Mousavi, M. S., et al., "Predictive torque control of induction motor based on a robust integral sliding mode observer," *IEEE Transactions on Industrial Electronics*, Vol. 70, No. 3, 2339–2350, Mar. 2023.
26. Yu, Y. and X. Liu, "Model-free fractional-order sliding mode control of electric drive system based on nonlinear disturbance observer," *Fractal and Fractional*, Vol. 6, No. 10, 603, 2022.
27. Zhang, Y., J. Jin, and L. Huang, "Model-free predictive current control of PMSM drives based on extended state observer using ultralocal model," *IEEE Transactions on Industrial Electronics*, Vol. 68, No. 2, 993–1003, 2021.
28. Gao, S., Y. Wei, D. Zhang, H. Qi, Y. Wei, and Z. Yang, "Model-free hybrid parallel predictive speed control based on ultra-local model of pmsm for electric vehicles," *IEEE Transactions on Industrial Electronics*, Vol. 69, No. 10, 9739–9748, 2022.
29. Li, T. and X. Liu, "Model-free non-cascade integral sliding mode control of permanent magnet synchronous motor drive with a fast reaching law," *Symmetry*, Vol. 13, No. 9, 1680, 2021.
30. Liu, H., W. Lin, Z. Liu, C. Buccella, and C. Cecati, "Model predictive current control with model-aid extended state observer compensation for PMSM drive," *IEEE Transactions on Power Electronics*, Vol. 38, No. 3, 3152–3162, 2023.